ACKNOWLEDGMENT

We would like to thank Barry A. Siegel, MD, for his guidance.

REFERENCES

1. Bane BL, Evans HL, Ro JY, et al. Extraskeletal osteosarcoma. *Cancer* 1990;65:2762–2770.
2. Kransdorf MJ, Meis JM. Extraskeletal osseous and cartilaginous tumors of the extremities. *Radiographics* 1993;13:853–884.
3. Peller PJ, Ho VB, Kransdorf MJ. Extraskeletal technetium-99m-MDP uptake: a pathophysiologic approach. *Radiographics* 1993;13:715–734.
4. Low-Beer BVA, Bell HG, McCorkle HJ, et al. Measurement of radioactive phosphorus in breast tumors in situ: a possible diagnostic procedure. *Radiology* 1946;47:492–493.
5. Whitley JE, Witcofski RL, Bolliger TT, et al. Technetium-99m in the visualization of neoplasms outside the brain. *Am J Roentgenol Radium Ther Nuklearmedizin* 1966;96:706–710.
6. Berg GR, Kalisher L, Osmond JD, Pendergrass HP, Potsaid MS. Technetium-99m diphosphonate concentration in primary breast carcinoma. *Radiology* 1973;109:393–394.
7. Ross McDougall I, Pistenma DA. Concentration of technetium-99m diphoshonate in breast tissue. *Radiology* 1974;112:655–657.
8. Hobbs S, Neumann RD, Merino MJ, Gunzenhauser J, Carascquillo JA. Localization of technetium-99m-MDP in cystosarcoma phyllodes. *Clin Nucl Med* 1992;17:58–60.
9. Serafini AN, Raskin MM, Zard LC, Watson DD. Radionuclide breast scanning in carcinoma of the breast. *J Nucl Med* 1974;15:1149–1152.
10. Piccolo S, Lastoria S, Mainolfi C, Muto P, Bazzicalupo L, Salvatore M. Technetium-99m-MDP scintamammography to image primary breast cancer. *J Nucl Med* 1995;36:718–724.
11. Waxman AD, Ramanna L, Memsic LD, et al. Thallium scintigraphy in the evaluation of mass abnormalities of the breast. *J Nucl Med* 1993;34:18–23.
12. Lee VW, Sax EJ, McAneny DB, et al. A complementary role for thallium-201 scintigraphy with mammography in the diagnosis of breast cancer. *J Nucl Med* 1993;34:2095–2100.
13. Waxman AD, Ashok G, Kooba A, et al. The use of technetium-99m-MIBI in evaluation of patients with primary carcinoma of the breast: comparison with thallium-201 [Abstract]. *J Nucl Med* 1993;34:(suppl):139P.
14. Khalkhali I, Cutrone JA, Mena IG, et al. Scintimammography: the complementary role of technetium-99m sestamibi prone breast imaging for the diagnosis of breast cancer. *Radiology* 1995;196:421–426.
15. Waxman A, Nagaraj N, Ashok G, et al. Sensitivity and specificity of technetium-99m-MIBI in the evaluation of primary carcinoma of the breast [Abstract]. *J Nucl Med* 1994;35:(suppl):22P.
16. Lastoria S, Varrella P, Mainolfi C, et al. Technetium-99m sestamibi scintigraphy in the diagnosis of primary breast cancer [Abstract]. *J Nucl Med* 1994;35:(suppl):22P.
17. Foschini MP, Dina RE, Eusebi V. Sarcomatoid neoplasms of the breast: proposed definitions for biphasic and monophasic sarcomatoid mammary carcinomas. *Semin Diag Path* 1993;10:128–136.
18. Wargotz ES, Norris HJ. Metaplastic carcinoma of the breast. I. Matrix-producing carcinomas. *Human Path* 1989;20:628–635.
19. Burnett KR, Lyons KP, Theron-Brown W. Uptake of osteotropic radionuclides in the breast. *Semin Nucl Med* 1984;14:48–49.
20. Worsley DF, Lentle BC. Uptake of technetium-99m-MDP in primary amyloidosis with a review of the mechanisms of soft-tissue localization of bone-seeking radiopharmaceuticals. *J Nucl Med* 1993;34:1612–1615.

Sentinel Node Imaging Via a Nonparticulate Receptor-Binding Radiotracer

David R. Vera, Erik R. Wisner and Robert C. Stadalnik

Department of Radiology, University of California, Davis, Medical Center, Sacramento, California

Technetium-99m-labeled polydiethylenetriamine pentaacetic acid polymannosyl polylysine (DTPA-*man*-PL) was synthesized and tested for lymph node scintigraphy by subcutaneous administration. The agent was designed for receptor-mediated uptake by mannose-binding protein, which resides on the plasma membrane of reticuloendothelial cells. **Methods:** Subcutaneous injections of a ^{99m}Tc-labeled agent having 18 DTPA and 82 mannosyl groups attached to a polylysine of 100 units ([^{99m}Tc]DTPA$_{18}$-*man*$_{82}$-PL$_{100}$) were made at the level of the metacarpus and metatarsus of three healthy rabbits. Images were acquired at 1, 6, 12 and 24 hr. Popliteal and axillary nodes were then assayed for percent of injected dose (%ID). A negative control study was performed in three normal rabbits with [^{99m}Tc]DTPA$_{18}$-PL$_{100}$. **Results:** Significant differences in mean 24-hr %ID between the receptor specific and nonspecific agents were observed for both the popliteal ($p < 0.006$) and axillary ($p < 0.012$) nodes. Popliteal percent injected dose at 24 hr was 3.00 ± 0.72% for [^{99m}Tc]DTPA-*man*-PL and 0.13 ± 0.08% for [^{99m}Tc]DTPA-polylysine. Axillary accumulation at 24 hr was 2.84 ± 0.83% for [^{99m}Tc]DTPA-*mannosyl*-polylysine and 0.22 ± 0.12% for [^{99m}Tc]DTPA-polylysine. Percent injected dose of the receptor-specific agent was highest (4%) during the 6-hr scan. Accumulation of the nonspecific agent by the popliteal and axillary nodes at 6-hr postinjection was approximately 0.5%. **Conclusion:** This study provides proof of principle for lymphoscintigraphy by receptor-mediated delivery of a nonparticulate imaging agent.

Key Words: lymphoscintigraphy; receptor-binding radiopharmaceutical; sentinel node imaging

J Nucl Med 1997; 38:530–535

Received Mar. 18, 1996; revision accepted Jul. 3, 1996.

For correspondence or reprints contact: David R. Vera, PhD, Division of Nuclear Medicine, Research I, Room 1001, 4635 2nd Ave., University of California, Davis, Medical Center, Sacramento, CA 95817.

Sentinel node imaging is a nuclear medicine examination that identifies the first lymph node to receive lymphatic flow from the primary tumor site. Because this node will be invaded first by malignant cancer cells, its removal and microscopic examination is an extremely sensitive index of metastatic disease (*1*). Also, using an intraoperative probe, sentinel node scintigraphy can be used as a basis for accurately detecting and excising regional lymph nodes for cancer staging (*2–6*). These procedures entail administering a particulate radiopharmaceutical intradermally or subcutaneously and localizing radiopharmaceutical uptake in targeted regional lymph nodes using a planar gamma camera as well as a gamma-probe intraoperatively at the time of staging lymphadenectomy. Advantages of these procedures include preoperative or intraoperative localization of the sentinel node which reduces extent of surgical intervention; verification of excision of the sentinel node increasing accuracy of cancer staging; and real-time detection of additional lymph nodes at the surgical site.

With the withdrawal of ^{99m}Tc-labeled antimony-trisulfide from the U.S. market, clinicians were left without an agent specifically designed for lymphoscintigraphy. Filtered ^{99m}Tc-sulfur colloid (*7,8*), ^{99m}Tc-labeled colloimdal albumin (*9*) and ^{99m}Tc-human serum albumin are used as replacements, but do not possess the attributes of an ideal sentinel node imaging agent. Such an agent would provide a 100% detection rate for the sentinel lymph node. The current agents do not achieve this goal. In patients with breast cancer, ^{99m}Tc-antimony-trisulfide (*10*) and unfiltered technetium-sulfur colloid have detection rates of 91% and 82%, respectively. Filtered technetium-sulfur colloid yields a detection rate of 84% in patients with melanoma (*11*). This rate was increased to 96% when both preoperative

lymphoscintigraphy and an intraoperative blue dye injection were used. This observation leads us to conclude that an ideal sentinel node imaging agent would have the injection site clearance of a dye and the retention time within the lymph node of a colloid. We, therefore, propose a new radiopharmaceutical based on receptor-binding technology which will permit optimization of imaging properties through rational chemical design (*12–14*).

Mannose-binding protein (MBP) belongs to a class of receptors called lectins (*15*). This receptor binds mannose-terminated glycoproteins (*16*) and is found in high densities in mammalian lung macrophages (*17*), liver nonparenchymal and parenchymal cells (*18*), serum (*19*) and lymphoid tissue (*20*). The receptor within lymph node tissue exhibits calcium-dependent binding within a within a pH range of 7–9 and demonstrates equal affinity for glycoproteins with carbohydrate sidechains that terminate with *N*-acetyl-mannosamine, *N*-acetylglucosamine, mannosamine or mannose.

As a first step toward the design of a sentinel node imaging agent, we report lymphoscintigraphy using a nonparticulate receptor-binding radiotracer. In this article, we propose the ideal properties of a sentinel node radiopharmaceutical and discuss the chemical attributes of a synthetic MBP ligand with which we will optimize sentinel node detection.

MATERIALS AND METHODS

Experimental Design

To demonstrate lymphoscintigraphy through MBP-mediated binding, we imaged healthy rabbits with the MBP analog ligand [^{99m}Tc]DTPA-*mannosyl*-polylysine. We also imaged rabbits with [^{99m}Tc]DTPA-polylysine. This molecule is not a MBP ligand, and therefore, served as a negative control. Additionally, we administered an amount of [^{99m}Tc]DTPA-*mannosyl*-polylysine that would saturate receptor sites within the sentinel node. This allowed us to approximate lymph node MBP density. This value will enable us to optimize the sentinel node uptake in future studies.

Synthesis

Polydiethylenetriamine pentaacetic acid polymannosyl polylysine (DTPA-*man*-PL) was synthesized in two steps: first, by covalent attachment of diethylenetriamine pentaacetic acid (DTPA) to polylysine (PL), and second, by covalent attachment of mannose to the remaining lysine residues of DTPA-PL. Coupling of DTPA to the polylysine backbone used the mixed anhydride method (*21*). The molar ratio of DTPA to poly-L-lysine hydrobromide polydispersity = 1.32, average mol wt = 20.9 kDa, degree of polymerization = 100) was approximately 12 to 1. After stirring overnight at room temperature, the organic solvents were removed by rotary evaporation. The product was then isolated by diafiltration with an ultrafiltration membrane having a molecular weight cutoff of 3 kDa. After 10 exchange-volumes of distilled water, the retentate was concentrated to 10 ml. The product was then filtered (0.45 μm) into a serum vial for lyophylization. The molecular weight and DTPA density were calculated as previously described (*22*). The product, $DTPA_{18}$-PL_{100}, had a molecular weight of 21.3 kDa and a DTPA density of 18 mol per mole of polylysine.

Conjugation of $DTPA_{18}$-PL_{100} with mannose was accomplished by reductive alkylation. The mannosyl coupling reagent, 3-oxypropy-2,3,4,6-tetra-*O*-acetyl-1-thio-β-D-mannoside, was synthesized by the following route. Tetra-*O*-acetyl-α-D-mannopyranosyl bromide was produced by a two-step reaction in chloroform (*23*). After rotary evaporation to a syrup, the product was immediately reacted with thiourea to produce 2-*S*-(2,3,4,6-tetra-*O*-actyl-β-D-mannopyranosyl)-2-peusdothiourea-hydrobromide (*24*), which was recrystallized in acetone. This product was derivatized with acrolein (*25*) and fractionated on a Sephadex LH-20 column (5 × 186 cm, 0.5 ml/min 95% ethanol) using the same elution parameters as 3-oxopropyl-tetra-*O*-acetyl-1-thiogalactoside (*26*). After rotary evaporation the product was stored as a clear syrup at −20°C. Deacetylation of 3-oxopropyl-tetra-*O*-acetyl-1-thiomannoside (50 m*M*) was performed at room temperature for 24 hr using sodium methoxide (40 m*M*) in freshly distilled methanol. After neutralization with 0.1 *M* acetic acid, 100 ml of the clear golden solution was transferred to a recovery flask and rotary-evaporated under reduced pressure. Coupling to $DTPA_{18}$-PL_{100} (100 mg) was conducted in 70 ml of phosphate buffer (0.2 *M*, pH 7.0) with 0.70 g of $NaCNBH_3$ (0.15 *M*) at 37°C while shaking for 20 hr. The molar ratio of coupling reagent to unconjugated lysine was 12.5 to 1. Unreacted coupling reagent was removed by diafiltration (molecular weight cutoff = 3 kDa) with 10 exchange volumes of distilled water. After concentration to 10 ml, the retentate was filtered (0.45 μm) into a glass serum vial and lyophylized. Measurement of mannose density and the molecular weight calculation used the method outlined for [Gd]DTPA-*gal*-PL (*22*).

Labeling

Technetium-99m labeling of both agents used a modification to a tin reduction method that has been previously described (*26*). Briefly, in a 2-ml glass vial fitted with a rubber septum, 1.6×10^{-7} mol of $DTPA_{18}$-man_{82}-PL_{100} or $DTPA_{18}$-PL_{100} in 0.50 ml of saline (0.9%) was combined with a 0.25-ml saline (0.9%) solution of sodium pertechnetate (50 mCi). After purging with nitrogen for 10 min, a fresh 0.10-ml solution of tin chloride (5.0 mg $SnCl_2$ in 0.175 ml of 37% HCl followed by 25 ml of 0.9% saline) was added and the reaction was allowed to stand for 90 min at room temperature. The product was then applied to a size-exclusion column (Sephadex G-10, 1 × 10 cm, 1.0 ml/min 0.9% saline), and the labeled product was collected during the second 1.5 min of elution. A similar column equipped with a flow-through gamma detector was used to measure the labeling yield. The concentration of the injectate was determined by UV absorption (225 nm) with a known concentration of $DTPA_{18}$-man_{82}-PL_{100} or $DTPA_{18}$-PL_{100} as the standard.

Imaging

Three normal adult New Zealand white rabbits were imaged with the receptor-binding radiotracer [^{99m}Tc]DTPA-*mannosyl*-polylysine, and three age and size-matched rabbits were imaged with a nonspecific radiotracer [^{99m}Tc]DTPA-polylysine. Each rabbit received a subcutaneous injection (0.05 ml, ~0.4 mCi, 2×10^{-8} mol) at the level of the metacarpus and metatarpus, bilaterally (total of four injection sites). Images were acquired (512 × 512 × 8, 500,000 cts) at 0.25, 1, 6 and 24 hr postinjection with the injection sites shielded with lead. Immediately after aquisition of the 24-hr image, each rabbit was euthanized and the popliteal and axillary lymph nodes were excised and assayed for radioactivity.

We calculated lymph node uptake in the following manner. The percent of injected dose (%ID) of each node was measured by counting (100–200 keV) the excised nodes with a known fraction of the administered dose. Regions of interest (ROI) were drawn around each node within the 0.25, 1, 6 and 24-hr images. Counts per minute within each ROI were determined, corrected for decay and background and converted to percent injected dose using the counting rate within each 24-hr ROI and the percent injected dose measured at 24 hr. One popliteal node from a [^{99m}Tc]$DTPA_{18}$-man_{82}-PL_{100} study could not be found at dissection. One popliteal node and two axillary nodes from the negative control study could not be found.

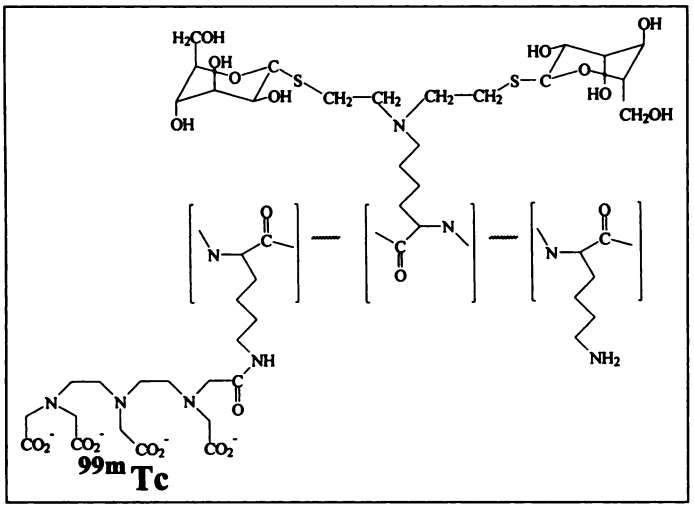

FIGURE 1. Technetium-99-labeled DTPA-*mannosyl*-polylysine is the synthetic ligand to the mannose-binding protein receptor. The conjugate used in this study was composed of a polylysine backbone of 100 lysines, 18 diethylenetriamine pentaacetic acid molecules complexed with ^{99m}Tc and 82 mannose groups which served as the receptor substrate.

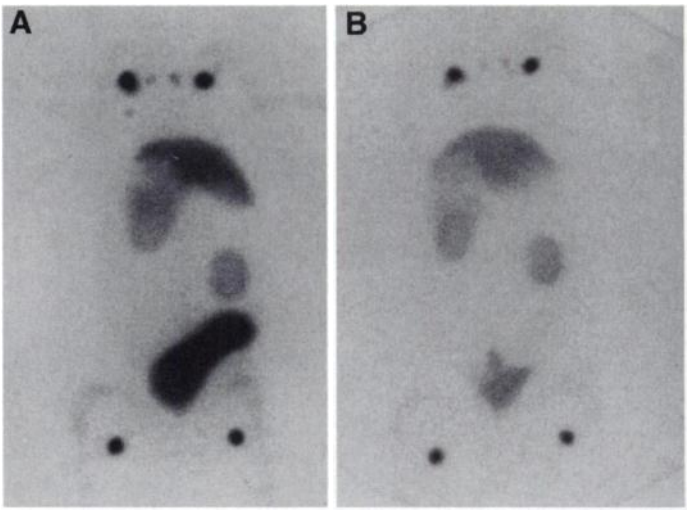

FIGURE 2. Whole body lymphoscintigrams of a normal rabbit obtained 6 (A) and 24 hr (B) after subcutaneous injection of [^{99m}Tc]DPTA-*mannosyl*-polylysine into all four distal extremities. There is significant activity in the axillary and popliteal lymph nodes. The injection sites were shielded.

Statistical Analysis

The unpaired Student's t-test was used to determine the p-level between the mean percent injected doses of the receptor-specific and the nonspecific radiotracers. A p level >0.05 was considered significant.

RESULTS

Synthesis

Figure 1 represents the receptor-specific agent [^{99m}Tc]DTPA-*mannosyl*-polylysine. The DTPA and mannose densities and molecular weight were 18 and 82 mol/mol of polylysine and 41.5 kDa, respectively. Typical labeling yields measured before size-exclusion chromatography were in excess of 98%. The specific activity was typically 0.03 Ci/μmol.

Imaging

Figures 2 and 3 are representative of the imaging study. Six hours after administration of the receptor-specific agent [^{99m}Tc]DTPA-*mannosyl*-polylysine, the first-order axillary nodes are easily visualized (Fig. 2A). The nodal activity persists up to 24 hr (Fig. 2B), indicating a receptor-specific interaction that is highly irreversible. The percent injected dose for the left popliteal, right popliteal, left axillary and right axillary nodes were 2.2%, 2.4%, 3.7% and 3.6%, respectively. At 6-hr postadministration of the nonspecific agent [^{99m}Tc]DTPA-polylysine, a faint impression of the nodes (Fig. 3B) is presumably due to the flow of radioactivity through the lymph channel and passive accumulation within intranodal lymph fluid; these processes peaked during the 0.25 and 1-hr scans. A nonspecific image at 24 hr is presented in Figure 3B. The percent injected dose for the left popliteal, right popliteal, left axillary and right axillary nodes were 0.26%, 0.21%, 0.46% and 0.47%, respectively.

Table 1 summarizes the percent injected dose for the popliteal and axillary nodes at 24-hr postadministration of the receptor-binding agent [^{99m}Tc]DTPA-*mannosyl*-polylysine and the nonspecific agent [^{99m}Tc]DTPA-polylysine, which being devoid of the receptor substrate (mannose) served as a negative control. Popliteal percent injected dose at 24 hr was 3.00 ± 0.72% for [^{99m}Tc]DTPA-*mannosyl*-polylysine and 0.13 ± 0.08% for [^{99m}Tc]DTPA-polylysine. Axillary accumulation at 24 hr was 2.84 ± 0.83% for [^{99m}Tc]DTPA-*mannosyl*-polylysine and 0.22 ± 0.12% for [^{99m}Tc]DTPA-polylysine. Accumulation of the nonspecific agent by the popliteal and axillary nodes at 6-hr postinjection was approximately 0.5% of the dose. The receptor-specific agent delivered over 10 times the radioactivity than the nonspecific radiotracer.

Significant differences in mean 24-hr percent injected dose between the receptor-specific and nonspecific agents were observed for both the popliteal ($p < 0.006$) and axillary ($p < 0.012$) nodes. The p levels for percent injected dose differences of the axillary nodes at 0.25, 1 and 6 hr postinjection were 0.738, 0.049 and 0.011, respectively. The p levels for the popliteal nodes were 0.007, 0.002 and <0.001 at 0.25, 1 and 6 hr.

Figure 4 is a plot of the mean percent injected dose within the popliteal and axillary nodes at 0.25, 1, 6 and 24 hr. Accumulation of the receptor-specific agent peaked at 4% during the 6-hr scan. Accumulation by the popliteal and axillary nodes of the nonspecific agent during the 6-hr scan was approximately 0.5%. Based on a maximum uptake of 4% of the injected [^{99m}Tc]DPTA-*mannosyl*-polylysine and a typical lymph node

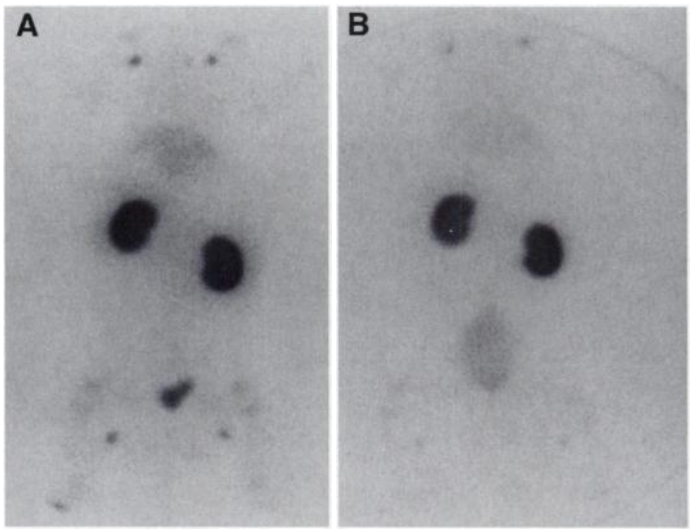

FIGURE 3. Whole-body lymphoscintigrams of a normal rabbit obtained 6 hr (A) and 24 hr (B) after subcutaneous injection of [^{99m}Tc]DTPA-polylysine into all four distal extremities. There is significantly less lymph node activity as compared with corresponding images of the previous figure. The injection sites were shielded.

TABLE 1
Percent Injected Dose at 24 Hours

Lymph node	Percent injected dose		p level
	[^{99m}Tc]DTPA$_{18}$-*man*$_{82}$-PL$_{100}$	[^{99m}Tc]DTPA$_{18}$-PL$_{100}$	
Popliteal	3.00 ± 0.72*	0.13 ± 0.08†	0.006
Axillary	2.84 ± 0.83‡	0.22 ± 0.15‡	0.012

*n = 6.
†n = 5.
‡n = 4.

weight of 0.2 g, the receptor density is approximately 4 nmol/g of lymphoid tissue.

This approximation assumes that 100% of the receptor sites were occupied. Although other lymph nodes were detected with ^{99m}Tc-DTPA-*man*-PL, the axillary and popliteal were the only nodes that were excised and assayed for radioactivity. There are no central nodes which receive afferent drainage from the axillary nodes. However, there are proximally located pelvic lymph nodes with afferent lymphatic communications from the popliteal nodes (*27*). Internal iliac node activity was identified if the urinary bladder was devoid of activity. These nodes, which are adjacent to the urinary bladder, were difficult to visualize and dissect when the bladder contained activity.

DISCUSSION

Our results demonstrate recognition and binding of a mannose-terminated macromolecule. Imaging and biodistribution measurements demonstrated lymph node uptake of [^{99m}Tc] DTPA-*mannosyl*-polylysine. Technetium-99m-labeled-DTPA-polylysine, which consisted of the same molecular backbone without carbohydrate sidechains, did not exhibit lymph node uptake. These data are consistent with the biochemical properties of the receptor MBP.

Sentinel node imaging has used two classes of imaging agents: radiolabeled particulates that bind to lymphoid tissue and radiolabeled macromolecules that provide node images as they flow through the lymph node chain. Sentinel node imaging of malignant melanoma originally used ^{198}Au-gold colloid (*28*), ^{99m}Tc-stannous phytate (*29*) and ^{99m}Tc-labeled dextran (*30*). Most nuclear medicine departments switched to ^{99m}Tc-antimony-trisulfide colloid when it became available through a Phase III company-sponsored IND. When ^{99m}Tc-antimony-trisulfide colloid was removed from the market in the U.S., ^{99m}Tc-labeled human serum albumin (TcHSA) (*6*), and various forms of filtered particulates, such as Millipore-filtered ^{99m}technetium-sulfur colloid (*7,8*), and filtered ^{99m}Tc-labeled colloidal albumin (*9*) were used. None of these agents, however, were designed specifically for sentinel node imaging. As a result, sentinel imaging with any of these agents suffers several deficiencies.

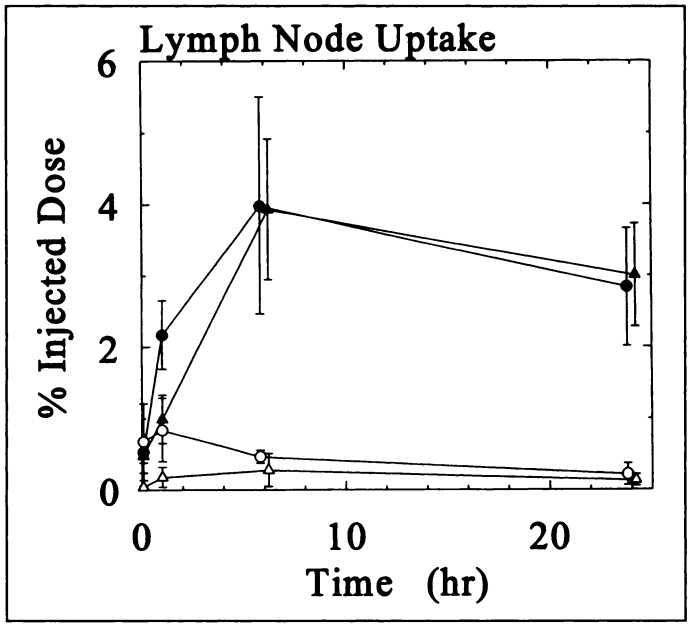

FIGURE 4. Percent injected dose versus time of the receptor-binding lymphotrophic imaging agent [^{99m}Tc]DTPA-*mannosyl*-polylysine (●, ▲) and a negative control [^{99m}Tc]DTPA-polylysine (○, △). The percent injected dose of the popliteal nodes (▲, △) were significantly different at all time points. The percent injected dose of the axillary nodes (●, ○) were significantly different at 1, 6 and 24 hr.

Filtered colloids and ^{99m}Tc-antimony-trisulfide colloids have mean diameters in the 1–10-nm range. These agents exhibit slow clearance from the injection site. The half-times for filtered TcHSA colloid and ^{99m}technetium-sulfur colloid are 5.5 and 10.5 hr, respectively (*31*). This translates to approximately 65% and 85% of the dose at the injection site at 3-hr postinjection, the optimal time for the intraoperative search for the sentinel node (*10*). Ege (*32*) reported a slow and highly variable injection site clearance of 1–35% over 24 hr. Labeled macromolecules have diameters within the same range but exhibit faster clearance (*31,33*). Technetium-99m-labeled-dextran (*33*) (molecular weight = 110 kDa) and Tc-HSA (*31*) (radius of gyration = 3.3 nm) have half-times of 0.5 and 2.8 hr, respectively. At physiologic pH, polylysines exist as random coils (*34*); consequently, both Tc-DTPA$_{18}$-*man*$_{82}$-PL$_{100}$ (molecular weight = 42 kDa) and Tc-DTPA$_{18}$-PL$_{100}$ (molecular weight = 21 kDa) have molecular dimensions (*35*) smaller than human serum albumin (molecular weight = 69 kDa).

Sentinel node extraction of ^{99m}Tc-antimony-trisulfide colloid and filtered particulates is not complete. Ege et al. (*36*) reported that the percentage of ^{99m}Tc-antimony-trisulfide colloid retained in all visualized nodes averaged less than 3% of the injected dose. In sentinel node imaging the typical nodal uptake is 4% (*37*); consequently, distal nodes also accumulate activity. The result can be confusing as to which of many nodes is the first in the chain. Therefore, the most frequently noted problem is that the timing of the intramammary tracer injection before surgery will have a significant effect on the number of nodes found intraoperatively (*10*). When multiple nodes are visualized, one cannot assume that the node nearest the tumor is the sentinel node (*38*); lymphatic vessels can bypass proximal nodes and then return to the node nearest the tumor. Static imaging of this anatomy using an agent with incomplete nodal extraction will produce a false-positive study. Dynamic imaging can mitigate this problem, however the best solution is an agent that completely accumulates within the sentinel node.

A less frequently encountered problem exists with the current agents. There are reports of severely diminished sentinel node uptake when the node has a high tumor burden (*39*). This can occur when radiopharmaceuticals of low specific activity are used. Filtered radiolabeled colloids will be susceptible to this problem. This stems from the fact that the overall radiochemical yield of these preparations ranges from 7% to 10%. Therefore, very high levels of pertechnetate (200–300 mCi) are required for a single dose. A receptor-binding agent, such as [^{99m}Tc]DTPA-*mannosyl*-polylysine can overcome this problem.

An optimal sentinel node imaging agent would deliver nearly 100% of the injected activity to the sentinel node. This would eliminate the need for a dynamic imaging study and prevent confusion with nonsentinel nodes during intraoperative detec-

tion. Complete clearance from the injection site would prevent the remaining activity from obscuring the sentinel node. Consequently, an ideal sentinel node imaging agent would exhibit the following properties: (a) rapid clearance from the injection site, (b) rapid, complete and sustained uptake by the sentinel lymph node, (c) low uptake by more distal second-order nodes and (d) a facile technetium-99m labeling system of high radiochemical purity and specific activity. The standard features of low radiation absorption, and high biological safety also apply. In reality, complete uptake by the first node within a chain will not occur; however, the distribution of a small fraction to the distal nodes could help identify the lymphatic anatomy.

We consider [^{99m}Tc]DTPA-*mannosyl*-polylysine as a prototype structure; its sole purpose was a demonstration of lymphoscintigraphy by targeting a receptor within lymphoid tissue. An optimized chemical structure will have a higher mannose density, and a higher specific activity than the agent used in this study. The backbone would be hydrophilic and produce an MBP ligand with an apparent size less than the current lymphoscintigraphic agents. These attributes would yield an agent with a rapid injection site clearance, similar to ^{99m}Tc-labeled dextran. Additionally, the backbone should provide an adequate number of attachment sites, which will determine the mannose and DTPA densities. These densities will control receptor affinity and specific activity, respectively. An imaging agent of high receptor affinity would have a high sentinel nodel extraction efficiency; and a high specific activity would permit injections of low molar dose and administration volume.

The molecular backbone will be the primary determinant of injection site clearance. Polylysine is linear and bears a net positive charge; the linearity reduces its apparent size (*40*) which increases diffusion. Polylysine, however, is extremely expensive. The other potential backbones are human serum albumin, dextran, synthetic copolymers (*41*) and starburst dendrimers (*42*). Dextran, a branched polymer of glucose, has an extensive human-use experience, and offers the highest ratio of attachment sites per molecular weight. It is also very hydrophilic; this feature makes it extremely effective in entering the lymph channel (*33*). Of the group, dextran is the least expensive. Numerous methods exist (*43*) for covalent attachment of various substrates to the hydroxyl units of polysaccarides. Synthetic copolymers offer linearity and a net neutral charge which also increases diffusion. Although the copolymers can be synthesized in bulk, there are many steps in the reaction sequence which significantly adds to their expense. Lastly, there is limited human-use experience with this backbone. Starburst dendrimers provide less molecular weight heterogeneity. Their disadvantage is that they offer the lowest number of attachment sites per backbone, and therefore may not provide an adequate density of mannose, and consequently may yield an agent of low receptor affinity.

The mannose density will control the sentinel node extraction efficiency and, as a result, accumulation of the tracer. A general feature of neoglycoconjugate binding to lectins (*44*) is that binding affinity is directly proportional to carbohydrate density of the ligand. More specifically, in vitro measurements of galactosyl-neoglycoalbumin binding (*12*) to its lectin, hepatic binding protein demonstrate that the forward binding rate constant increases with higher galactose density, while the reverse binding rate constant does not change. It is the forward binding rate constant that controls the extraction efficiency of a receptor-binding agent (*45*). The ability to chemically control the forward binding rate constant is a critical feature of an imaging agent that does not recirculate through the target tissue. Therefore, uptake of a lymphoscintigraphic agent depends on the ability of the tissue to extract the agent during a single passage through the node.

Indirect labeling of the neoglycoconjugate through DTPA yields an extremely stable product of high-specific activity and radiochemical purity. Using a 30-min incubation time we routinely label DTPA-*galactosyl*-polylysine (*26*) with radiochemical purities in excess of 98% and specific activities of 100 Ci/μmol. At this specific activity the administration of a 1-mCi dose would require 0.01 nmol of receptor for complete binding of the agent at the sentinel node. Depending on the species, tissue densities of mammalian lectins (*15*) are in the range of 0.5–1.0 nmol/g of tissue. Studies of rat lymphoid tissue indicate that MBP density is at the high end of this range (*20*). This value is similar to our density measurement of 4 nmol/g MBP. Therefore, a 0.01-nmol injection will occupy less than 1% of the receptor sites within a 1-g lymph node. As a result, a MBP ligand should be capable of delivering 100% to a node that was replaced with 90% tumor.

Our goal is to achieve a sentinel node imaging agent with increased diagnostic performance at a lower cost than the current lymphoscintigraphic agents. We envision a tin-based kit, which achieves a quantitative labeling yield after a 30-min incubation at room temperature. The preparation would be stable for many hours and would, therefore, provide for multiple studies. Rapid and complete injection site clearance would permit early imaging and the possibility of SPECT scanning if desired. High sentinel node extraction would eliminate the need for dynamic imaging, which would reduce camera and technologist time. Most importantly, this same property would also increase the specificity of intraoperative sentinel node detection. Lastly, it may be possible to incorporate a dye into the ligand structure. This would permit visual guidance during resection of the sentinel node.

CONCLUSION

This study provides a proof of principle that a nonparticulate radiotracer can successfully image lymph nodes through receptor-specific uptake by MBP. Unlike particulate agents, MBP radioligands offer greater chemical flexibility for the rational design of a sentinel node imaging agent. It is our hypothesis that such a radiopharmaceutical will provide higher diagnostic performance at substantially reduced expense over current sentinel node imaging with ^{99m}Tc-labeled colloids.

ACKNOWLEDGMENTS

We thank Mr. Dusan P. Hutak for his excellent technical assistance. This work was supported in part by University of California Breast Cancer Research Program grant 2RB-0118 and U.S. Public Health Service grant AM04758.

Presented at the 43rd Annual Meeting of the Society of Nuclear Medicine.

REFERENCES

1. Morton DL, Wen D-R, Wong JH, et al. Technical details of intraoperative lymphatic mapping for early stage melanoma. *Arch Surg* 1992;127:392–399.
2. Alex JC, Krag DN. Gamma-probe guided localization of lymph nodes. *Surg Oncol* 1993;2:137–143.
3. Krag DN, Weaver JC, Alex JC, Fairbank JT. Surgical resection and radiolocalization of the sentinel lymph node in breast cancer using a gamma probe. *J Surg Oncol* 1993;2:335–340.
4. Uren RF, Howman-Giles RB, Thompson JF, et al. Lymphoscintigraphy to identify sentinel lymph nodes in patients with melanoma. *Melanoma Res* 1994;4:395–399.
5. van der Veen H, Hoekstra OS, Paul MA, Cuesta MA, Meijer S. Gamma probe-guided sentinel node biopsy to select patients with melanoma for lymphadenectomy. *Br J Surg* 1994;81:1769–1970.
6. Krag DN, Meijer SJ, Weaver DL, et al. Minimal-access surgery for staging of malignant melanoma. *Arch Surg* 1995;130:654–658.
7. Sacks GA, Sandler MP, Born ML. Lymphoscintigraphy as an adjunctive procedure in the perioperative assessment of patients undergoing microlymphaticovenous anastomoses. *Clin Nucl Med* 1983;8:309–311.

8. Hung JC, Wiseman GA, Wahner HW, Mullan BP, Taggart TR, Dunn WL. Filtered technetium-99m-sulfur colloid evaluated for lymphoscintigraphy. *J Nucl Med* 1995; 36:1895–1901.
9. Pijpers R, Collet GJ, Meijer S, Hoekstra OS. The impact of dynamic lymphoscintigraphy and gamma probe guidance on sentinel node biopsy in melanoma. *Eur J Nucl Med* 1995;22:1238–1241.
10. Uren RF, Howman-Giles RB, Thompson JF, et al. Mammary lymphoscintigraphy in breast cancer. *J Nucl Med* 1995;36:1775–1780.
11. Albertini JJ, Cruse CW, Rapaport D, et al. Intraoperative radiolymphoscintigraphy improves sentinel lymph node identification for patients with melanoma. *Ann Surg* 1996;223:217–224.
12. Vera DR, Krohn KA, Stadalnik RC, Scheibe PO. Technetium-99m galactosyl-neoglycoalbumin: in vivo characterization of receptor-mediated binding. *J Nucl Med* 1984;25:779–787.
13. Stadalnik RC, Vera DR, Woodle ES, et al. Technetium-99m NGA functional hepatic imaging: preliminary clinical experience. *J Nucl Med* 1985;26:1233–1242.
14. Vera DR, Stadalnik RC, Kudo M, Krohn KA. Radiopharmaceutical preparation of technetium-99m-galactosyl-neoglycoalbumin. *Methods Enzymol* 1994;247:402–408.
15. Steer CJ, Ashwell G. Receptor-mediated endocytosis: mechanisms, biologic function, and molecular properties. In: Zakim D, Boyer TD, eds. *Hepatology: a textbook of liver disease*, 2nd ed. Philadelphia: W.B. Saunders; 1990:137–182.
16. Achord DT, Brot FE, Sly WS. Inhibition of the rat clearance system for agalacto-orosomucoid by yeast mannans and by mannose. *Biochem Biophys Res Commun* 1977;77:409–415.
17. Stahl PD, Rodman JS, Miller MJ, Schlesinger PH. Evidence for receptor-mediated binding of glycoproteins, glycoconjugates and lysosomal glycosidases by alveolar macrophages. *Proc Natl Acad Sci USA* 1978;75:1399–1403.
18. Praaning-Van Dalen DP, DeLeeuw AM, Brouwer A, Knook DL. Rat liver endothelial cells have a greater capacity than Kupffer cells to endocytose *N*-acetylglucosamine- and mannose-terminated glycoproteins. *Hepatology* 1987;7:672–679.
19. Kozutsumi Y, Kawasaki T, Yamashina I. Isolation and characterization of a mannan-binding protein from rabbit serum. *Biochem Biophys Res Commun* 1980;95:658–665.
20. Kawasaki T, Mizuno Y, Masuda T, Yamashina I. Mannan-binding protein in lymphoid tissues of rats. *J Biochem (Tokyo)* 1980;88:1891–1894.
21. Krejcarek GE, Tucker KL. Covalent attachment of chelating groups to macromolecules. *Biochem Biophys Res Commun* 1977;77:581–583.
22. Vera DR, Buonocore MH, Wisner ER, Katzberg RW, Stadalnik RC. A molecular receptor-binding contrast agent for magnetic resonance imaging of the liver. *Acad Radiol* 1995;2:497–507.
23. Kőrösy F, Bárczai-Martos M. Preparation of acetobrome-sugars. *Nature* 1950;165: 369.
24. Chipowsky S, Lee YC. Synthesis of 1-thioaldosides having an amino group at the aglycon terminal. *Carbohydr Res* 1973;31:339–346.
25. Lee RT, Lee YC. Preparation of new ω-aldehydroalkyl 1-thio-D-glycopyranosides and their coupling to bovine serum albumin by reductive alkylation. *Carbohydr Res* 1982;101:49–55.
26. Vera DR, Topcu S, Stadalnik RC. In vitro quantification of asialoglycoprotein receptor density from human hepatic microsamples. *Methods Enzymol* 1995;247:394–402.
27. Barone R, Pavaux C, Blin PC, Cuq P. *Atlas d'anatomie du lapin*. Paris: Masson; 1973:129–143.
28. Robinson DS, Sample WF, Fee HJ, Holmes EC, Morton DL. Regional lymphatic drainage in primary malignant melanoma of the trunk determined by colloidal gold scanning. *Surg Forum* 1977;28:147–148.
29. Alavi A, Staum MM, Sheosl FB, Bloch PH. Technetium-99m-stannous phytate as an imaging agent for lymph nodes. *J Nucl Med* 1978;19:422–426.
30. Bennett LR, Lago G. Cutaneous lymphoscintigraphy in malignant melanoma. *Semin Nucl Med* 1983;13:61–69.
31. Glass EC, Essner R, Giuliano A, Morton DL. Comparative efficacy of three lymphoscintigraphic agents. *J Nucl Med* 1995;36:199P.
32. Ege NG. Internal mammary lymphoscintigraphy. *Radiology* 1976;118:101–107.
33. Henze E, Schelbert HR, Collins JD, Najafi A, Barrio JR, Bennett LR. Lymphoscintigraphy with ^{99m}Tc-labeled dextran. *J Nucl Med* 1982;23:923–929.
34. Doty P, Imahori K, Klemperer E. The solution properties and configurations of a polyampholytic polypeptide: copoly-L-lysine-L-glutamic acid. *Proc Natl Acad Sci USA* 1958;44:424–431.
35. Tanford C. *Physical chemistry of macromolecules*. New York: John Wiley & Sons Inc.; 1961.
36. Ege E, Warbick-Cerone A, Bronskill MJ. Radionuclide lymphoscintigraphy-an update. In: Sodd VJ, Hoogland DR, Allen DR, Ice RD, Sorenson JA, eds. *Radiopharmaceuticals II. Proceedings of the 2nd International Symposium on Radiopharmaceuticals*. New York: Society of Nuclear Medicine; 1979:241–258.
37. Kapteijn BAE, Panday RKLB, Liem IH, et al. Lymphoscintigraphy and intraoperative gamma probe detection of the first draining lymph node in clinically localized melanoma. *J Nucl Med* 1995;36:222P.
38. Taylor S, Murray D, Herd S, Vansant J, Alazraki N. The importance of dynamic lymphoscintigraphy in detecting the sentinel node. *J Nucl Med* 1995;36:223P.
39. Giuliano AE, Kirgan DM, Guenther JM, Morton DL. Lymphatic mapping and sentinel lymphadenectomy for breast cancer. *Ann Surg* 1994;220:391–401.
40. Seymour LW. Passive tumor targeting of soluble macromolecules and drug conjugates. *Crit Rev Ther Drug Carrier Syst* 1992;9:135–187.
41. Krinick NL, Rihová B, Ulbrich K, Strohalm J, Kopecek J. Synthesis of *N*-(2-hydroxypropyl)methacrylamide copolymer-anti-Thy 1.2 antibody-chlorin e_6 conjugates and a preliminary study of their photodynamic effect on mouse splenocytes *in vitro*. *Makromol Chem* 1990;191:839–856.
42. Tomalia DA, Baker H, Deward J, et al. A new class of polymers: starburst-dendritic macromolecules. *Polymer J* 1985;17:117–132.
43. Molteni L. Dextrans as drug carriers. In: Gregoriadis G, ed. *Drug carriers in biology and medicine*. San Diego: Academic Press; 1979:107–125.
44. Lee YC. Neoglycoconjugates: general considerations. In: Lee YC, Lee RT, eds. *Neoglycoconjugates: preparation and applications*. San Diego: Academic Press; 1994:3–21.
45. Vera DR, Krohn KA, Scheibe PO, Stadalnik RC. Identifiability analysis of an in vivo receptor-binding radiopharmacokinetic system. *IEEE Trans Biomed Engr* 1985; 32:312–322.

FIRST IMPRESSIONS

Is this a normal liver? For acquisition information, see page 643.